Conference Proceedings

Solar World Congress 2015
Daegu, Korea, 08 – 12 November 2015

Experimental Validation of a Compound Parabolic Concentrator Mathematical Model

García-Valladares O.[2], Santos-González I.[1], Gómez V.H.[2], Ortega N[2].

[1]Posgrado en Ingeniería (Energía), Universidad Nacional Autónoma de México, Privada Xochicalco s/n, Temixco, Morelos 62580, México. irsag@ier.unam.mx

[2]Instituto de Energías Renovables, Universidad Nacional Autónoma de México, Privada Xochicalco s/n, Temixco, Morelos 62580, México. ogv@ier.unam.mx

Abstract

In this work the numerical simulation and experimental validation of a Compound Parabolic Concentrator (CPC) are presented. The numerical model solve the governing equations of continuity, momentum and energy inside the CPC receiver tube, together with the energy equation in the receiver tube wall and the thermal analysis in the solar concentrator. The model can predict the increment of temperature between the inlet and outlet section of the CPC, the thermal efficiency and the pressure drop through the CPC together with the flow variables (mass flow rate, temperature and pressure) in each control volume in which the CPC is divided.

A prototype of a CPC has been designed and built using a cylindrical receiver with a real concentration rate of 1.8, acceptance angle of 30°, and aperture area of 0.17 m^2.

The protocol ANSI-ASHRAE 93-1986 standard was used with appropriate instrumentation for measuring the different variables in the CPC. For this prototype experimental tests were performed using water as working fluid for a wide range of inlet water temperatures and mass flow rates.

Statistical analysis was carried out in order to compare variations between the experimental results and numerical results. According to the results, the numerical model provides good tendencies for the design and optimization of CPCs.

key-words*: solar energy, CPC, numerical model, characterization curves, statistical analysis*.

Nomenclature

A_a	Receiver tube heat transfer area, [m^2]
A_c	Cover heat transfer area, [m^2]
A_r	Reflector heat transfer area [m^2]
A_t	Fluid flow cross section area [m^2]
D_{in}	Internal diameter [m]
e	Specific energy ($h+v^2/2+gz \sin\theta$) [J/kg]
f	Friction factor [dimensionless]
g	Gravitational constant [9.81 m/s^2]
h	Enthalpy [J/kg]
h	Heat transfer coefficient [$W/(m^2K)$]
I	Solar irradiance [W/m^2]
K	Thermal conductivity [W/mK]
m	Mass [kg]
$\dot{m}$	Mass flow rate [kg/s]
P	Pressure [Pa]
p	Perimeter [m]
q	Heat flow per unit area [W/m^2]

doi:10.18086/swc.2015.10.03 Available at http://proceedings.ises.org

q_u	Heat flux per receiver unit area from fluid to wall [W/m^2]
r	Radius of the receiver tube [m]
T	Temperature [°C]
$\vec{V}$	Velocity in the axial direction [m/s]
v	velocity [m/s]
x	Axial coordinate

Greek letters

β	Inclination angle of receiver tube [degree]
γ	Length of tangent [m]
ε	Emittance [dimensionless]
θ	Angle of incidence on collector [degrees]
θc	Half-acceptance angle [degrees]
ρ	Density [kg/m^3]
σ	Stefan-Boltzman constant (5.6697x10^{-8}W/m^{2}K^4)
τ_w	Wall shear stress (N/m^2)
Δt	Temporal discretization step [s]
ΔT	Temperature difference [°C]
Δx	Spatial discretization step [m]
Φ	Two-phase frictional multiplier [dimensionless]

Subscripts

a	Receiver tube
amb	Ambient
c	Cover
conv	Convective
f	Fluid
g	Gas
in	Inlet
j	Number of control volume
l	Liquid
r	Reflector
rad	Radiative
sky	Sky
tp	Two-phase

Superscripts

-	Arithmetical average over a control volume
~	Integral average over a control volume
$[X]_{j-1}^{j}$	Difference between the variable X at the outlet section and the inlet section.

1. Introduction

The alternative to reduce dependence on fossil fuels and the amount of CO2 emitted into the atmosphere is the use of renewable energies. Water is generally heated by commercial fuels (LP gas, natural gas, electricity) in urban areas to be used for space heating, domestic or industrial processes. The majority of commercial fuels are directly or indirectly produced by fossil fuels which have limited reserves and contribute greatly to the global warming. The integration of renewable energy systems will utilize clean and sustainable energy to reduce the dependence of fossil fuels and provide long term energy savings.

Solar energy collectors transform solar radiation into heat and then transfer this heat to a fluid. The compound parabolic concentrator (CPC) is a versatile solar collector due to the amount of applications and geometries that can be used. The CPC is a good choice for applications in direct evaporation or water heating near its boiling point, because these stationary collectors have a good quality rate between cost and performance at medium temperature levels [1]. The CPC could be used in a great variety of solar applications for low and medium temperature ranges; the most important is the heat production for industrial processes, such as sterilization, pasteurization, drying, distillation, adsorption and absorption cooling, etc.

CPCs consist basically of three elements: receiver, cover and reflector. In order to achieve good CPC performance, a numerical model is a useful tool in order to design it. In this work a numerical model of the CPC was carried out; then a CPC was designed and built selecting carefully the geometry and material of each component. Appropiate instrumentation was selected and used in order to compare the experimental data of the CPC under different working conditions with the model results in order to validate it.

2. CPC Design

The design of the reflector portion of a CPC tubular receiver (Figure 1) is determined by the diameter of the receiver and the desired concentration factor. The reflector geometry is given in two separate parts:

An involute section $|\theta| < \theta_c + \pi/2$ and a segment of a parabola $|\theta| > \theta_c + \pi/2$

$$\gamma(\theta) = r\theta \quad \text{for} \quad |\theta| \leq \theta_c + \frac{\pi}{2} \quad \text{(Involute)}$$

$$\gamma(\theta) = \left[r \frac{\theta + \theta_c + \frac{\pi}{2} - \cos(\theta - \theta_c)}{1 + \sin(\theta - \theta_c)} \right] \quad \text{for} \quad \theta_c + \frac{\pi}{2} \leq |\theta| \leq \frac{3\pi}{2} - \theta_c$$

The curve is generated by increasing θ in radians, calculating the length γ and the X,Y coordinates.

$$x = r \sin\theta - \gamma \cos\theta$$
$$y = -r \cos\theta - \gamma \sin\theta$$

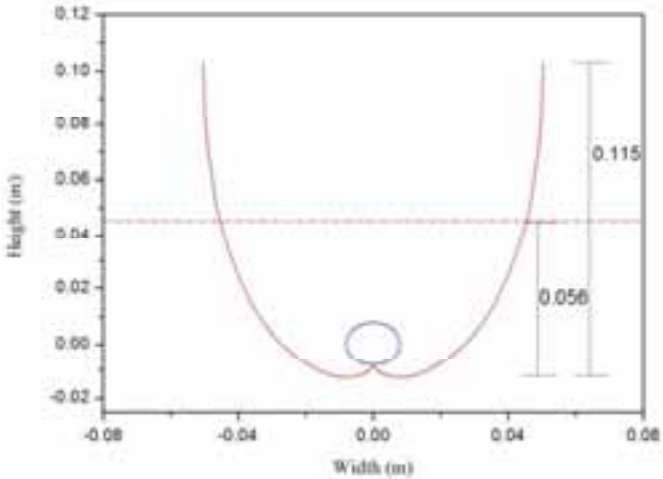

Figure 1. A CPC tubular receiver design.

In practical applications the upper part of the reflector are less efficient to reflect solar rays to the receiver. For this reason, it is truncated and the cost of reflective material is reduced. Table 1 shows the percentage of material saved when truncation is applied.

Table 1. Truncated and non-truncated final designs.

	Non-truncated (m)	Height truncated (m)	% Reduction
Height	0.115	0.056	51
Aperture	0.100	0.090	10
Reflector perimeter	0.281	0.163	42.1

3. Numerical model

The CPC was designed using a one-dimensional numerical model that solves the governing equations of continuity, momentum and energy. The fluid flow inside the receiver tube, the heat conduction in the receiver tube wall, and the heat transfer in the solar concentrator were solved in a segregated manner. For

more detailed of the numerical model see N. Ortega, et. al. [2] .

Figure 2 shows a control volume in CPC and the energy balances in each component (receiver tube, cover and reflector, Fig 2a) together with a control volume for the fluid flow (Fig 2b)

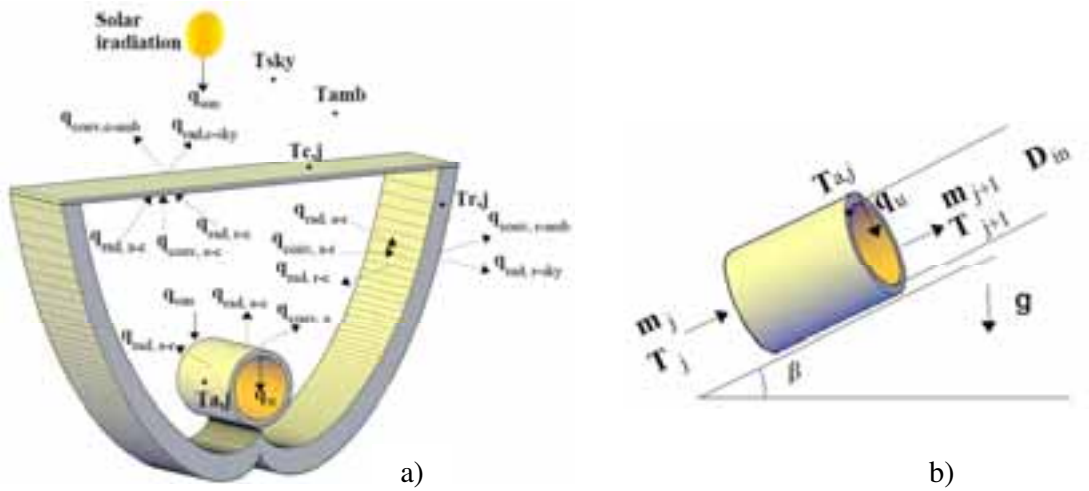

Figure 2. A CPC control volume. a) energy balance in each component; b) the fluid flow control volume.

For the fluid flow inside the receiver tube (see Fig 2b), the following governing equations have been integrated using a control volume analysis and a step by step method in the flow direction.

Continuity:

$$[\dot{m}]_{j-1}^{j} + \frac{\partial m}{\partial t} = 0 \tag{1}$$

The mass flow rate is obtained from the discretized continuity equation: $\dot{m}_j = \dot{m}_{j-1} - \frac{A_t \Delta x}{\Delta t}\left(\bar{\rho}_{tp} - \bar{\rho}_{tp}^{o}\right)$ (2)

Momentum:

$$\left[\dot{m}_g V_g + \dot{m}_l V_l\right]_{j-1}^{j} + \Delta x \frac{\partial \bar{m}}{\partial t} = -[P]_{j-1}^{j} A_t - \tilde{\tau}_w p_{Ar.j} \Delta x - mgsin\beta \tag{3}$$

The discretized momentum equation is solved for the outlet pressure:

$$P_j = P_{j-1} - \frac{\Delta x}{A_t}\left\{\pi D_{in} \Phi \frac{\bar{f}}{4} \frac{\bar{m}^2}{2\rho_{tp} A_t^2} + \left[\frac{\dot{m}}{\Delta x}\left(x_g \vec{V}_g + \left(1 + x_g\right)\vec{V}_l\right)\right]_{j-1}^{j} + \frac{\bar{m} - \bar{m}^o}{\Delta t} + \rho_{tp} A_t g sin\beta\right\} \tag{4}$$

Energy:

$$\left[m_l e_l + m_g e_g\right]_{j-1}^{j} + \frac{\partial(\bar{m}_l \bar{e}_l + \bar{m}_g \bar{e}_g)}{\partial t} - A_t \Delta x \frac{\partial \bar{P}}{\partial t} = \tilde{q}_u p \Delta x \tag{5}$$

From the energy equation and the continuity equation, the following is obtained for the outlet enthalpy:

$$h_j = \frac{(2\pi D_{in} \Delta x) q_u - a\dot{m}_j + b\dot{m}_{j-1} + cA_t \Delta x / \Delta t}{\dot{m}_j + \dot{m}_{j-1} + \bar{\rho}_{tp}^{o} A_t \Delta x / \Delta t} \tag{6}$$

Where:

$$q_u = h_f\left(T_{a,j} - (\bar{T}_j + \bar{T}_{j+1})/2\right) \tag{7}$$

$$a = \left[x_g \vec{V}_g + \left(1 - x_g\right)\vec{V}_l\right]_j^2 + gsin\beta\Delta x - h_{j-1} \tag{8}$$

$$b = \left[x_g \vec{V}_g + \left(1 - x_g\right)\vec{V}_l\right]_j^2 + gsin\beta\Delta x + h_{j-1} \tag{9}$$

$$c = 2\left(\overline{P}_{j-1} - \overline{P}^{o}_{j-1}\right) - \overline{\rho}^{o}_{tp}\left(\mathrm{h}_{j-1} - 2\overline{\mathrm{h}}^{o}_{j-1}\right) - \left(\overline{\rho}\vec{V}^{2}_{j-1} - \overline{\rho}^{o}\vec{V}^{o\,2}_{j-1}\right) \tag{10}$$

The discretized equations are coupled using a fully implicit step by step method in the flow direction. From the known values at the inlet section and the wall boundary conditions, the variable values at the outlet of each CV are iteratively obtained from the discretized governing equations. Outlet values are the inlet values for the next CV. The procedure is carried out until the end of the receiver tube is reached.

The heat conduction in the receiver tube wall has been written assuming one-dimensional transient temperature distribution. A characteristics CV is shown in Figure 3, where P represents the central node, E and W indicate its neighbors. The CV faces are indicated by e, w, n, and s. Integrating the energy equation over this CV, the following equation was obtained.

$$\left((\tilde{\mathrm{q}}_{\mathrm{sun}} - \tilde{q}_{rad,a-c} - \tilde{q}_{rad,a-r} - \tilde{q}_{conv,a})\mathrm{P_n} - \tilde{\mathrm{q}}_{\mathrm{u}}\mathrm{P_s}\right)\Delta\mathrm{x} + (\tilde{\mathrm{q}}_{\mathrm{w}} - \tilde{\mathrm{q}}_{\mathrm{e}})\mathrm{A}_t = \mathrm{m}\frac{\partial\tilde{\mathrm{h}}}{\partial\mathrm{t}} \tag{11}$$

here $\tilde{\mathrm{q}}_{\mathrm{u}}$ was evaluated using the convective heat transfer coefficient and temperature in the fluid flow and receiver wall temperature in each CV, and the conductive heat fluxes are evaluated from the Fourier law: $\tilde{\mathrm{q}}_{\mathrm{e}} = \mathrm{k}_{\mathrm{e}}(\partial\mathrm{T}/\partial\mathrm{x})_{\mathrm{e}}$ and $\tilde{\mathrm{q}}_{\mathrm{w}} = \mathrm{k}_{\mathrm{w}}(\partial\mathrm{T}/\partial\mathrm{x})_{\mathrm{w}}$

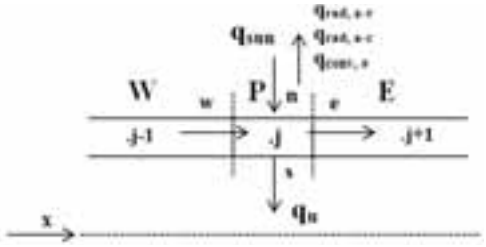

Figure 3. CV for the receiver tube wall.

The useful energy gain (q_u) is equal to the cover incident solar energy reduced by optical losses in the concentrator, the thermal losses in the cover, the reflector, and the receiver tube.

In order to calculate the receiver tube, cover and reflector temperatures in each CV; it is necessary to solve iteratively the following equations of energy balance of each component:

Receiver: $q_{sun,a} - q_{rad,a-c} - q_{rad,a-r} - q_{conv,a-c} - q_{conv,a-r} - q_u = 0$ (12)

Cover: $q_{abs,c} + q_{rad,a-c} + q_{conv,a-c} + q_{rad,r-c} - q_{conv,c-env} - q_{rad,c-sky} = 0$ (13)

Reflector: $q_{abs,r} + q_{rad,a-r} + q_{conv,a-r} - q_{rad,r-c} - q_{conv,r-env} - q_{rad,r-sky} = 0$ (14)

With equation (12, 13 and 14), the following equations are obtained:

$$T_r = \frac{(h_{rad,a-r}+h_{conv,a-r})T_a + h_{conv,r-amb}T_{amb} + h_{rad,r-sky}T_{sky} + (h_{conv,r-c}-h_{ra,r-c})T_c}{h_{rad,a-r}+h_{conv,a-r}+h_{conv,r-amb}+h_{rad,r-sky}+h_{conv,r-c}-h_{ra,r-c}} \tag{15}$$

$$T_c = \frac{(h_{rad,a-c}+h_{conv,a-c})T_a + h_{rad,c-sky}T_{sky} + h_{conv,c-amb}T_{amb} + (h_{conv,r-c}-h_{ra,r-c})T_r}{h_{rad,a-c}+h_{conv,a-r}+h_{rad,c-sky}+h_{conv,c-amb}+h_{conv,r-c}-h_{ra,r-c}} \tag{16}$$

$$T_a = \frac{(h_{rad,a-c}+h_{conv,a-c})T_c + (h_{conv,a-r}+h_{ra,a-r})T_r + q_{sun,a} - q_u}{h_{rad,a-c}+h_{conv,a-c}+h_{conv,a-r}} \tag{17}$$

The convective heat transfer coefficient between the receiver tube and the reflector and between the receiver tube and cover were expressed by [3]:

$$h_{conv,a-r} = 3.25 + 0.0085\frac{(Ta-Tr)}{2D_{out}} \quad (18)$$

$$h_{conv,a-c} = 3.25 + 0.0085\frac{(Ta-Tc)}{2D_{out}} \quad (19)$$

$$h_{rad,r-c} = \frac{\sigma\left(T_c^2+T_r^2\right)(T_c+T_r)}{(1-\varepsilon_c)/\varepsilon_c+((1-\varepsilon_r)/\varepsilon_r)(A_c/A_r)}\frac{A_r}{A_a} \quad (20)$$

$$h_{rad,c-sky} = \varepsilon_c\sigma(T_c^2 + T_{sky}^2)(T_c + T_{sky})\frac{A_c}{A_a} \quad (21)$$

$$h_{rad,r-sky} = \varepsilon_r\sigma(T_r^2 + T_{sky}^2)(T_r + T_{sky})\frac{A_r}{A_a} \quad (22)$$

$$h_{rad,a-c} = \frac{\sigma\left(T_a^2+T_c^2\right)(T_a+T_c)}{(1/\varepsilon_c)+(A_c/A_a)((1/\varepsilon_a)-1)} \quad (23)$$

$$h_{rad,a-r} = \frac{\sigma\left(T_a^2+T_r^2\right)(T_a+T_r)}{(1-\varepsilon_r)/\varepsilon_r+((1-\varepsilon_a)/\varepsilon_a)(A_r/A_a)} \quad (24)$$

The convective heat transfer coefficients between the cover and the ambient and between the reflector and the ambient are expressed by Duffie and Beckman [4]:

$$h_{conv,c-amb} = (5.7 + 3.8v)\frac{A_c}{A_a} \quad (25)$$

$$h_{conv,r-amb} = (5.7 + 3.8v)\frac{A_r}{A_a} \quad (26)$$

The numerical model can predict the increment of temperature between the inlet and outlet of the collector, the efficiency, the energy gain by the transport fluid and the pressure drop of the CPC together with the flow variables (mass flow rate, temperature and pressure) in each control volume in which the CPC is divided. The numerical model can be used with fluid mixtures and with or without phase change in the fluid flow.

4. Experimental setup

Figure 4 shows the CPC designed and built. The real concentration is 1.8, acceptance angle is 30° and aperture area of 0.17 m^2. Table 2 shows the characteristics of geometry and materials used in the construction of this CPC.

Figure 4: CPC designed and built.

Table 2: Geometrical characteristics and materials used for the CPC

Parameter	Characteristics
Cover	
Low-iron tempered glass	transmittance=0.91
Thickness (mm)	4
Reflector	
Anodized aluminum	reflectance=0.90
Thickness (mm)	0.35
Receiver	
Copper	½" nominal diameter
Internal/ external Diameter (mm)	14.5/15.9
Selective surface	absorptance=0.90
CPC	
Acceptance angle (°)	30
Maximum concentration	2.00
Real concentration ratio	1.80
Width (m)	0.090
Height (m)	0.057
Length (m)	1.95

An experimental setup was constructed (Figure 5). Proper instrumentation to control and register the different variables of the system together with a program to save the experimental data was developed. The following variables are register every 3 second in experimental tests: temperatures, global solar irradiance at the collector plane and mass flow rate. The instrumentation used and their uncertainties for the evaluation of CPC are shown in Table 3.

Figure 5. Experimental unit.

Table 3: Instrumentation

	Instrument	Operating range	Uncertainties
Temperature meter	Thermistor	-40 a 150°C	±0.1°C
	K-type thermocouple	-20 a 750°C	±1.1°C
Mass flow meter	Coriolis	0 a 20 kg/min	±0.1%
Radiation meter	Pyranometer-class II	285 a 2800 nm	±1%

5. Experimental tests

The tests were carried out in the Solar Platform of the Instituto de Energías Renovables of the Universidad Nacional Autónoma de México, located at Temixco, Morelos, México, at 18°50.36' N and at 99°14.07' W, with an altitude of 1219 m above sea level. In Temixco, the yearly average ambient temperature and solar irradiance on the horizontal plane are 23.1 °C and 20.05 MJ/m^2 day, respectively.

The collector is mounted on the support structure and the collector angle is set according to the day of the year of the test. CPC mass flow rate and inlet temperature were maintained constant with the recirculation loop, pump, and electrical heaters installed in the storage tank for cold water. The water coming from the CPC was stored in the hot water storage tank. The water in the hot water storage tank was returned with the recirculation pump to the cold water storage tank to fix a new temperature and mass flow rate to repeat the process.

The experimental tests were performed using water as working fluid at solar noon. The mass flow rate, inlet and outlet temperature at the collector, the ambient temperature and the irradiance at the collector plane were registered every 3 seconds.

6. Results

Figure 6 shows the thermal efficiency against the temperature difference between fluid inlet temperature and ambient temperature in relation with the solar irradiance at the CPC plane. The experimental and numerical results with a mass flow rate of 0.7 kg/min and 1.0 kg/min are shown. The errors bars in figures represent the uncertainty obtained in the experimental measurement.

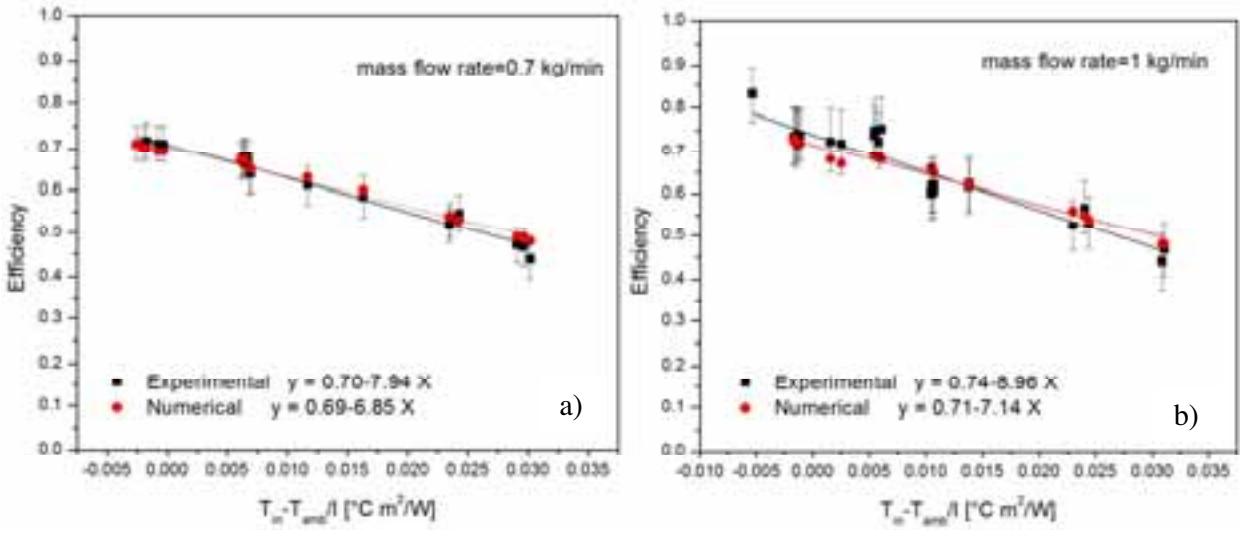

Figure 6. Numerical and experimental thermal efficiency results with a mass flow rate of: a) 0.7 kg/min and b) 1.0 kg/min.

The error and standard deviation between the experimental data and numerical results are shown in Table 4.

Table 4. Comparison between experimental and numerical results for the thermal efficiency.

Mass flow rate (kg/min)	Efficiency	
	Error (%)	Standard deviation (%)
0.7	±2.5	±1.9
1.0	±4.5	±3.2

Figure 7 shows the comparison of the increment of temperature through the CPC between the numerical results and experimental data for two different mass flow rate.

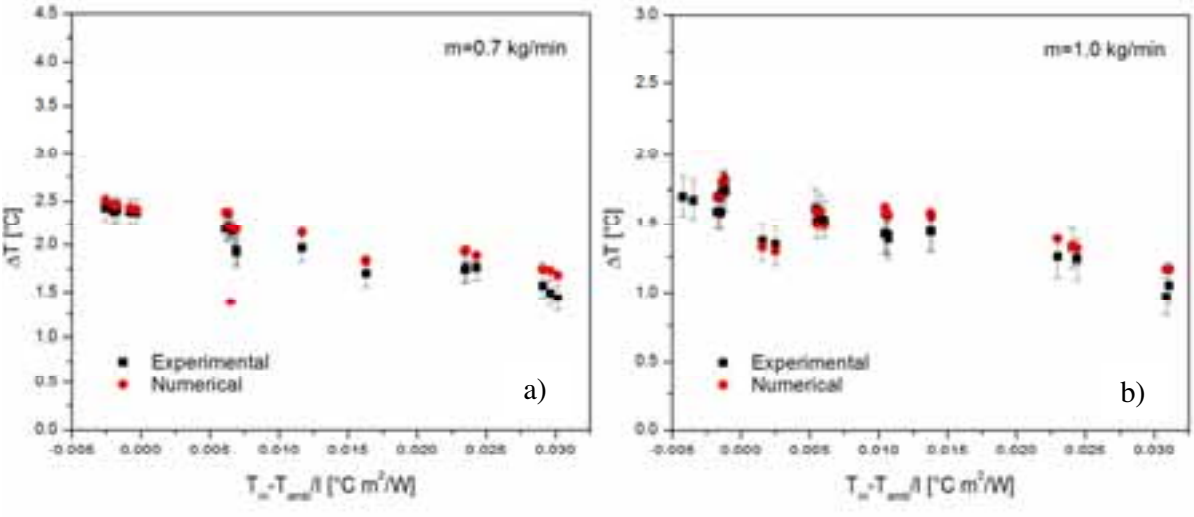

Figure 7. Comparison of the increment of temperature through the CPC between the experimental and numerical results for a mass flow rate of: a) 0.7 kg/min and b)1.0 kg/min.

The error and standard deviation between the experimental data and numerical results are shown in Table 5

Table 5. Comparison between experimental and numerical results for the increment of temperature.

Mass flow rate (kg/min)	ΔT	
	Absolute error (°C)	Standard deviation (°C)
0.7	±0.10	±0.06
1.0	±0.17	±0.17

7. CONCLUSIONS

The numerical model developed is based on the applications of governing equations and used empirical correlations. The numerical algorithm solves in a segregated manner the subroutines: heat conduction in the receiver tube wall, fluid flow inside the receiver tube and the useful energy gain in the solar concentrator.

A prototype of CPC with a real concentration of 1.8 and aperture area of 0.17 m^2 was designed and built. The experimental and numerical results were compared in order to validate the model.

Numerical model has proven to be reliable and was validated with experimental data of the CPC. The results have been satisfactory. The comparison between the experimental and numerical results shows that the numerical model provides good results and tendencies.

REFERENCES

[1] Collares-Pereira M. CPC type collectors and their potential for solar energy cooling applications. Proceedings of the Second Munich Discussion Meeting on Solar Assisted Cooling with Sorption Systems, Munchen, 1995, paper No. 5.
[2] Ortega N, García-Valladares O, Best R, Gómez VH. Two phase flow modelling of a solar concentrator applied as ammonia vapour generation in an absorption refrigerator. Renewable Energy 2008; 33:2064-2076
[3]Hsieh, C.K. Thermal analysis of CPC collectors, Solar Energy 1981; 27:19-29.
[4]Duffie, J.A., Beckman, W.A. Solar engineering of thermal processes, 2nd Ed. New York: Wiley Interscience, 1991; 174–354.

ACKNOWLEDGEMENTS

This work was partially supported by the following projects: PAPIIT project IT100812-3, FORDECYT project 190603, SENER-CONACyT project 117914 and CEMIE-Sol project 12.